RSC Advances

PAPER

View Article Online
View Journal | View Issue



Cite this: *RSC Adv.*, 2018, **8**, 21745

# 1,3,4-Thiadiazol derivative functionalized-$Fe_3O_4$@$SiO_2$ nanocomposites as a fluorescent probe for detection of $Hg^{2+}$ in water samples

Noshin Mir, *[a] Sara Jalilian,[a] Pouya Karimi,[a] Massoud Nejati-Yazdinejad[a] and Somaye Khammarnia[b]

Received 22nd April 2018
Accepted 24th May 2018

DOI: 10.1039/c8ra03448f

rsc.li/rsc-advances

5-Amino-1,3,4-thiadiazole-2-thiol was used to synthesize a novel fluorescent functionalizing group on a $Fe_3O_4$@$SiO_2$ magnetic nanocomposite surface for detection of heavy metal ions in water samples. The prepared probe was characterized by using X-ray diffraction, transmission electron microscopy, Fourier transform infrared spectroscopy, and a vibrating sample magnetometer. Among various tested ions, the new nanocomposite responded to $Hg^{2+}$ ions with an intense fluorescence "turn-off". The limit of detection of the probe shows that it is sensitive to the minimum $Hg^{2+}$ concentration of 48.7 nM. Theoretical calculations were done for estimating binding energies of the three possible bonding modes and the visualized molecular orbitals were presented.



## Introduction

The widespread toxicological properties of mercury have made it one of the most dangerous pollutants in the environment. Mercury released from natural sources or human activities ends up in the atmosphere and in water. According to the U.S. Environmental Protection Agency (EPA), the anthropogenic mercury emission in the US was measured to be 1.2 tons in 2011.[1,2] Methyl mercury, which usually bioaccumulates in fish, can cause serious neurotoxic damage to the body. On the other hand, the possible form of mercury in drinking water is inorganic mercury. The main target of inorganic mercury in the body is the kidneys and especially the proximal tubule where mercury is accumulated by either luminal uptake of Cys–S–Hg–S–Cys or by basolateral uptake.[3] The limit of mercury(II) concentration in drinking water has been determined by the EPA to be 2 ppb.[4]

In order to ascertain the exact amount of mercury ions in drinking water, there are various analytical methods including atomic absorption spectroscopy,[5] inductively coupled plasma-mass spectrometry,[6] high performance liquid chromatography,[7] and electrochemical sensing.[8] However, these techniques suffer from complex and unhandy equipment which limits their on-site applications. Recently, fluorescent probes have emerged as a novel, selective, clean, simple, and portable alternative for detection of various chemical compounds in different mediums.[9–13] Designing metal fluorescent probes is a challenging field of research since it needs a vast knowledge of metal coordination chemistry as well as photophysical mechanisms. Although designing new organic fluorophores is still of great importance, development of nanostructured substrates is more appealing since they serve a porous structure for hosting large amounts of fluorophore molecules and are conveniently separated after metal adsorption.[14]

The immobilization of organic fluorophores has been reported on certain nanosized substrates such as graphene quantum dots,[15] carbon dots,[16] Ag@$SiO_2$,[17] $SiO_2$,[18] MCM-41,[19] SBA-15,[20] and $Fe_3O_4$@$SiO_2$.[21] The privilege of easy separation with external magnetic field has made $Fe_3O_4$@$SiO_2$ a superior choice. Many reports have already presented application of different fluorescence probes based on $Fe_3O_4$@$SiO_2$ nanocomposites in detection and removal of heavy metals.[11,12,22–28] Both conventional and novel organic ligands with two important characteristics are potential for this purpose: (i) possessing suitable functional groups on one side to react and attach to $SiO_2$ surface either directly or through spacers such as (3-aminopropyl)triethoxysilane (APTES) or *N*-(2-amino ethyl)-3-aminopropyl trimetoxysilane (AEAPTES) (ii) having a fluorophore group which tends to coordinate with heavy metal and its fluorometric response changes after coordination. 1,3,4-thiadiazole has been known as a widely applied chemical compound in agricultural, pharmaceutical, and materials chemistry.[29] The broad spectrum of its biological activities in terms of antibacterial, anticancer, antidepressant, *etc.* has made it an attractive compound for biologists and chemists. The special structure of thiadiazole class of components enables keto/enol tautomerism which is the origin of fluidity of biological membranes,[30,31] crystal polymorphism, solvatomorphism effects, and interactions in lipid membranes.[32,33] Moreover, the dual fluorescence effect of 1,3,4-thiadiazole is an interesting phenomena which is very important in understanding protein interactions of this molecule in biological systems.[34]

[a]*Department of Chemistry, University of Zabol, P. O. Box 98615-538, Zabol, Islamic Republic of Iran. E-mail: n.mir@uoz.ac.ir; Fax: +985431232186; Tel: +985431232186*
[b]*Department of Chemistry, Payame Noor University, Iran*

Recently, our group reported the successful design of two novel $Fe_3O_4$@$SiO_2$ fluorescence probes with precise detection ability of mercury ion in water.[35,36] In continuation of our previous works, here, a novel fluorescent probe is designed and grafted on the $Fe_3O_4$@$SiO_2$ surface. A thiadiazole derivative is synthesized and applied as the fluorophore functionalizing group on $Fe_3O_4$@$SiO_2$ nanocomposites and is used for detection of $Hg^{2+}$ in drinking water. 5-Amino-1,3,4-thiadiazole-2-thiol (ATT) ligand which is used as a starting material in this work, has already been reported as a potential silica modifier for sorption of different heavy metals including $Hg^{2+}$.[37] The –SH site on the aromatic ring in this molecule has provided an excellent coordination ability to soft heavy metals.

## Experimental

### Characterization

X-ray diffraction (XRD) patterns were recorded by a Philips-X'PertPro, X-ray diffractometer using Ni-filtered Cu Kα radiation at scan range of $10° < 2\theta < 80°$. Scanning electron microscopy images were obtained on LEO-1455VP. Room temperature photoluminescence properties were studied on a Perkin-Elmer (LS 55) Mvv fluorescence spectrophotometer. Fourier transform infrared (FT-IR) spectra were recorded on Magna-IR, spectrometer 550 Nicolet with 0.125 $cm^{-1}$ resolution in KBr pellets in the range of 400–4000 $cm^{-1}$. TEM images were taken on an EM208S Philips transmission electron microscope with an accelerating voltage of 100 kV. For TEM analysis, the nanoparticle powder was dispersed in ethanol by ultrasonic bath. Then a drop of the dispersion was placed on the TEM grid and was dried in the vacuum oven and then it was used for TEM imaging. Room temperature magnetic properties were investigated using a vibrating sample magnetometer (VSM), made by Meghnatis Daghigh Kavir Company (Iran) in an applied magnetic field sweeping between ±10 000 Oe.

### Synthesis of thiadiazol-based ligand

5-(4-Vinylbenzylidene)amino-1,3,4-thiadiazole-2-thiol (VBYT) (3) was prepared using ATT by the classical Schiff base reaction. First, terephthaldialdehyde (TPAL) (1 mmol) was suspended in 10 mL of methanol and added to 5-amino-1,3,4-thiadiazole-2-thiol (1 mmol) and the solution was stirred under reflux at 100 °C for 1 h (VBYT, see Scheme 1). Then, AEAPTES (1 mmol) was added to this solution and the reaction mixture was stirred under reflux at 60 °C for another 1 h. The precipitate was filtered off and recrystallized in DMF. The red product (VBYT–AEAPTES, see Scheme 2) was then dried at room temperature. The progress of the reaction was checked by thin layer chromatography (TLC).

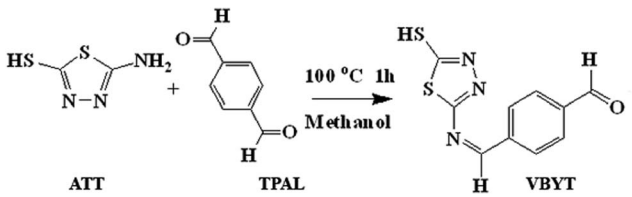


Scheme 1 Synthetic procedure of VBYT.

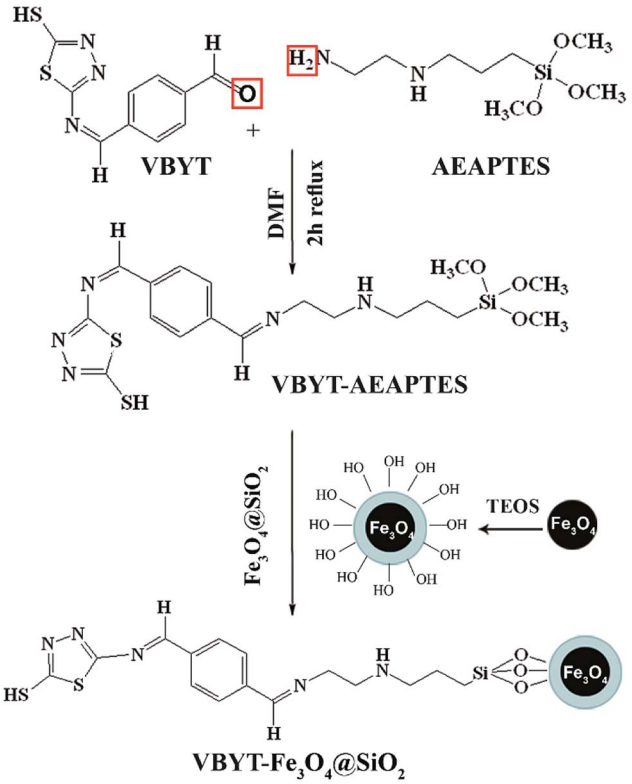


Scheme 2 The procedure for synthesis of VBYT-$Fe_3O_4$@$SiO_2$.

### Synthesis of magnetic $Fe_3O_4$@$SiO_2$ nanoparticles (NPs)

The $Fe_3O_4$-coated $SiO_2$ nanoparticles were synthesized by a similar procedure developed by Dong *et al.*[38] At first, for degassing the flask, the deionized water was exposed to nitrogen gas for 10 min. Then, $Fe(NO_3)_3 \cdot 9H_2O$ (8.12 g, 0.020 mol) and $FeCl_2 \cdot 4H_2O$ (2.00 g, 0.010 mol) and 1 mL oleic acid were dissolved in 30 mL deionized water at 90 °C under nitrogen atmosphere and vigorous mechanical stirring (1000 rpm). Then, 20 mL of $NH_4OH$ (28 wt%) was quickly injected into the reaction mixture in one portion and it immediately changed to black. The mixture continued under this condition (90 °C) for 2.5 h and the colloid solution was cooled to room temperature. After cooling, it was suspended in chloroform.

For preparation of $Fe_3O_4$@$SiO_2$ nanoparticles, a modified method reported by Zhu *et al.*[23] was used. 25 mg of $Fe_3O_4$ nanoparticles was added into 40 mL of cyclohexane at room temperature by ultrasonic dispersion. Triton X-100 (9 g), octanol (8 mL) and $H_2O$ (1.7 mL) were then added with stirring to form water-in-oil microemulsion. The reaction mixture was vigorously stirred for 15 min. Then, 1 mL of TEOS was added slowly into the solution. The reaction vessel was stirred on a shaker for 1.5 h at room temperature and then, 1 mL aqueous ammonia (28 wt%) was added into the reaction. The stirring continued for 24 h at room temperature to form the $Fe_3O_4$@$SiO_2$ core–shell nanoparticles. The $Fe_3O_4$@$SiO_2$ nanoparticles were isolated *via* centrifugation at 4000 rpm and washed with ethanol for five times. The obtained dark grey product was allowed to dry at 80 °C.

### Preparation of VBYT-$Fe_3O_4$@$SiO_2$

First, 30 mg of dried $Fe_3O_4$@$SiO_2$ and 30 mg (1 mmol) of VBYT–AEAPTES ligand were suspended in 20 mL of DMF. DMF was used as solvent here, because the solubility test for VBYT–AEAPTES ligand showed that it is completely soluble in it. The mixture was refluxed for 12 h at 60 °C. The products were collected by filtration and repeatedly washed with DMF and then ethanol several times.

### Preparation of the fluorometric metal ion titration solution

The fluorometric measurements of metal ions were performed in phosphate-buffered saline (PBS) solutions (0.02 M, pH = 7.0). 0.03 g of the functionalized $Fe_3O_4$@$SiO_2$ nanoparticles were dispersed in 3 mL of $1 \times 10^{-6}$ M of different metal nitrate ($Hg^{2+}$, $Na^{+}$, $Mg^{2+}$, $Ca^{2+}$, $Al^{3+}$, $Cr^{3+}$, $Zn^{2+}$, $Ni^{2+}$, and $Fe^{3+}$) aqueous PBS buffer solutions for testing the effect of metal type on fluorescence response of the as-prepared probe. The performance of the prepared nanocomposite was also tested in tap water of the chemistry laboratory located in University of Zabol, as a real sample.

### Calculations

The molecular structure of VBYT–AEAPTES and its interaction with $Hg^{2+}$ in three different bonding modes in the ground state were optimized on the basis of density function theory (DFT) at the Becke3–Lee–Yang–Parr (B3LYP) (with LanL2DZ basis) and by means of visual inspection using the GAUSSVIEW program (Version 5.0). All the calculations were performed using the GAUSSIAN 09 software package.[39] The population analysis was performed by natural bond orbital (NBO) method using NBO program[40] implemented under Gaussian 09 program package.[41]

## Results and discussion

### Characterization of as-prepared samples

The phase of the samples were characterized by their X-ray diffraction patterns. Fig. 1a and b show the XRD patterns of $Fe_3O_4$ and $Fe_3O_4$@$SiO_2$ nanoparticles, respectively. Fig. 1a shows that the pattern corresponds to pure cubic $Fe_3O_4$ with JCPDS card no.: 19-629. The XRD pattern of $Fe_3O_4$@$SiO_2$ consists of $SiO_2$ and $Fe_3O_4$ phases (Fig. 1b). The broad band at *ca.* $2\theta = 20$–$30°$ is attributed to the amorphous phase of $SiO_2$. The peaks corresponding to $Fe_3O_4$ in $Fe_3O_4$@$SiO_2$ (Fig. 1b) are weaker than those in pure $Fe_3O_4$ which shows that $Fe_3O_4$ is covered with $SiO_2$ shell.

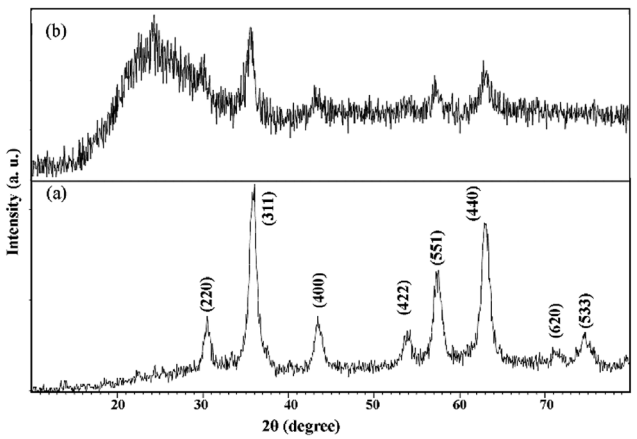


Fig. 1 XRD patterns of (a) $Fe_3O_4$ nanoparticles and (b) $Fe_3O_4$@$SiO_2$.

In order to study the surface chemistry of the samples, FT-IR spectroscopy was used. Fig. 2a–c show the FT-IR spectra of VBYT–AEAPTES ligand, $Fe_3O_4$@$SiO_2$, and VBYT-$Fe_3O_4$@$SiO_2$, respectively. In Fig. 2a, the weak peak at 712.86 $cm^{-1}$ is referred to C–S stretching vibration. The peak at 1060.18 $cm^{-1}$ is attributed to Si–O stretching vibration. The characteristic bands at 1610.43 and 1554.68 $cm^{-1}$ are attributed to C=N and C=C stretching vibrations, respectively. The extremely weak band at 2598.26 $cm^{-1}$ is for S–H stretching vibration.[42] The appeared peak at 2925.59 $cm^{-1}$ is assigned to $sp^3$ C–H stretching of alkane chain. A single vibration at 3342.17 $cm^{-1}$ is assigned to secondary amine in AEAPTES counterpart.

In Fig. 2b and c, the main appeared peaks correspond to $Fe_3O_4$ cores and $SiO_2$ shells. The peaks around 590 $cm^{-1}$ and 470 $cm^{-1}$ in Fig. 2b and c are assigned to the Fe–O vibration of magnetite core. The displayed bands around 3400 $cm^{-1}$ and 1636 $cm^{-1}$ are due to the stretching and bending vibration of remained $H_2O$ and silanol O–H groups, respectively. In both spectra, the broad and strong peak around 1100 $cm^{-1}$ is assigned to the overlapped stretching vibration of Si–O–Si bonds. Two characteristic peaks at 2854 $cm^{-1}$ and 2925 $cm^{-1}$ are referred to the symmetric and asymmetric stretching vibration of C–H of the alkyl groups. In Fig. 2c, weak peaks in the range of 1000–1700 $cm^{-1}$ show the attachment of VBYT–AEAPTES ligand on the surface of $Fe_3O_4$@$SiO_2$ nanocomposites.

For characterization of the prepared core–shell nanocomposites, TEM analysis was performed on images of VBYT-$Fe_3O_4$@$SiO_2$ sample and the results were shown in Fig. 3a and b. It can be seen that the formed nanoparticles are very tiny and are

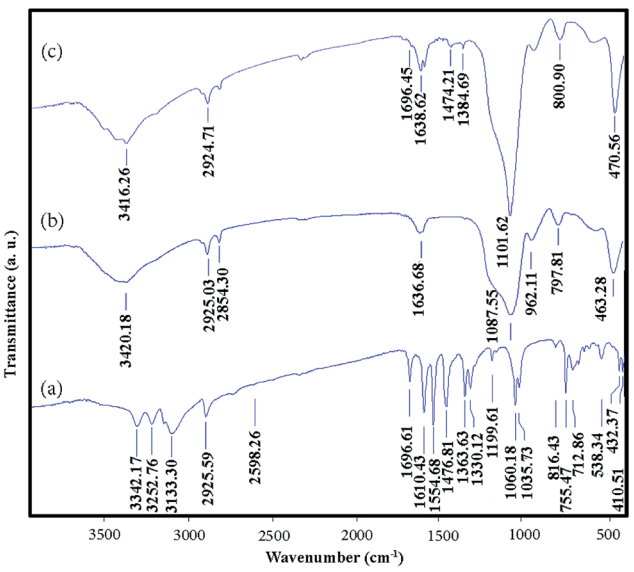


Fig. 2 FT-IR spectra of (a) VBYT–AEAPTES ligand, (b) $Fe_3O_4$@$SiO_2$, and (c) VBYT-$Fe_3O_4$@$SiO_2$.

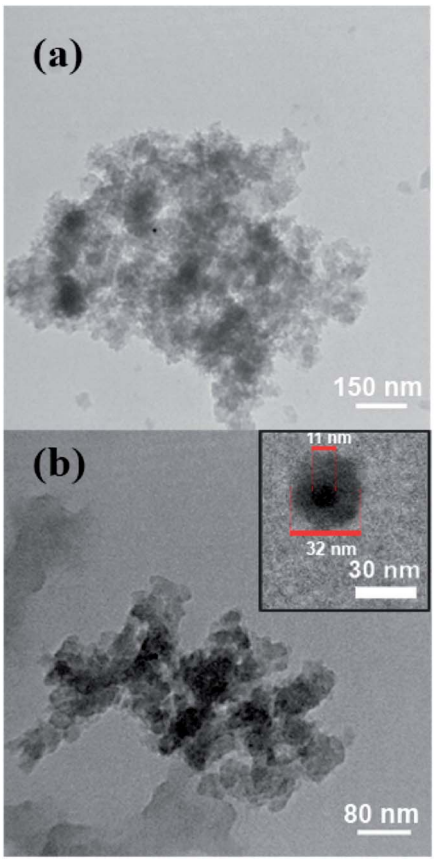


Fig. 3 (a) and (b) TEM images of VBYT-$Fe_3O_4$@$SiO_2$ from two different parts of the samples. Inset: one separate core–shell VBYT-$Fe_3O_4$@-$SiO_2$ nanoparticle.

partly agglomerated because of the magnetic properties of the nanocomposites. A higher magnification of one separate nanoparticle, shown in Fig. 3b-inset, clearly shows the core–shell structure of the nanocomposite. The diameter of the nanocomposite particle is approximately 32 nm with a core with the diameter of 11 nm. Therefore, the $SiO_2$ coverage layer around $Fe_3O_4$ core is about 21 nm.

For studying the magnetic properties of the $Fe_3O_4$ and VBYT-$Fe_3O_4$@$SiO_2$ a vibrating sample magnetometer was used at 300 K (Fig. 4). The measured saturation magnetizations (Ms) are 50.33 emu $g^{-1}$ and 2.89 emu $g^{-1}$ for $Fe_3O_4$ and VBYT-$Fe_3O$@$SiO_2$, respectively that are shown in Fig. 4a. This decrease in magnetic properties is due to coverage of the $Fe_3O_4$ cores by $SiO_2$ and VBYT layers. Both samples are superparamagnetic because they almost show no remanence and coercivity. Although the magnetization of VBYT-$Fe_3O$@$SiO_2$ is small, it is easily separated from the solution by placing a magnet, within 3 minutes (Fig. 4b). This results show that the prepared material is potential for water purification applications since it is efficiently absorbed by a simple magnet.

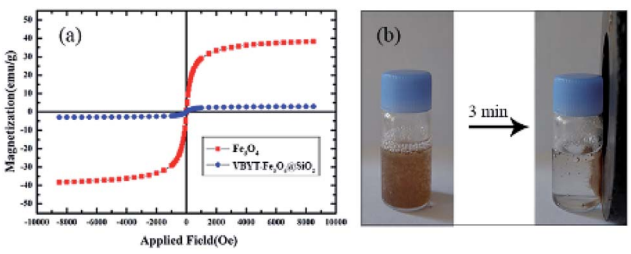


Fig. 4 (a) The magnetic hysteresis loops of $Fe_3O_4$@SiO and VBYT-$Fe_3O_4$@$SiO_2$ (b) the separation of VBYT-$Fe_3O_4$@$SiO_2$ in aqueous solution after 3 minutes.

## Testing the fluorescence properties of the nanocomposite in response to metal absorption

In order to test the response of the prepared sample against different metal ions, the fluorescence spectra of the nanocomposite were recorded in presence and absence of the some important metal ions including $Ni^{2+}$, $Hg^{2+}$, $Zn^{2+}$, $Mg^{2+}$, $Al^{3+}$, $Na^{+}$, $Ca^{2+}$, $Fe^{3+}$, and $Cr^{3+}$. Fig. 5 shows the results of the fluorescence test after exciting the samples at $\lambda_{exc}$ = 268 nm. The $\lambda_{max}$ emission ($\lambda_{max}$ em) of the free receptor (FR) *i.e.* VBYT-$Fe_3O_4$@-$SiO_2$ dispersed in buffer solution in absence of metal ions is at 409 nm. After addition of fixed amounts of $Hg^{2+}$, $Cr^{3+}$, $Ni^{2+}$, $Zn^{2+}$, $Mg^{2+}$, $Fe^{3+}$, $Al^{3+}$, $Ca^{2+}$, and $Na^{+}$ the intensity of the maximum peak was either unchanged or slightly tuned in case of $Al^{3+}$, $Ni^{2+}$ and $Ca^{2+}$. Moreover, almost no peak shift was observed at $\lambda_{max}$ em compared to the FR. For $Zn^{2+}$, the peak at 340 nm was intensified that probably could be attributed to its different bonding mode compared with other metal ions which prohibits the photoinduced electron transfer (PET) mechanism and results in a "turn-on" switching.[43,44] In case of $Hg^{2+}$, a significant quenching (about 1100 units) was observed for $\lambda_{max}$ em peak at 409 nm. Therefore, by comparing the response of VBYT-$Fe_3O_4$@$SiO_2$ nanocomposite to different ions, it was shown that the prepared material could be a good candidate for detection of $Hg^{2+}$ ions. Similar results have been reported for application of silica gel modified with ATT by Tzvetkova *et al.* They indicated that among some heavy metals including Cu(II), Co(II), Ni(II), Cd(II), Pb(II) and Hg(II), the modified silica gel shows the highest sorption capacity against Hg(II).[37] Certain factors such as suitable coordination geometry of ligand and ion, nitrogen affinity, and ion size and charge are effective in high selectivity of an ion.[35,45] In continue, more tests were

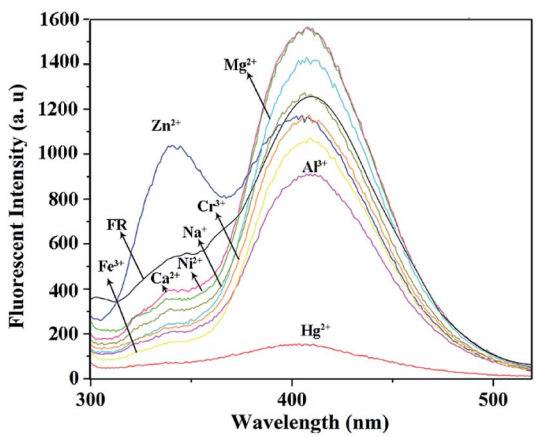


Fig. 5 The fluorescence spectra of VBYT-$Fe_3O_4$@$SiO_2$ in presence of various metal ions ($\lambda_{exc}$ = 268 nm).

conducted in order to show the potential application of the nanocomposite on detection of $Hg^{2+}$ ions in water samples.

To elucidate the detection potential of VBYT-$Fe_3O_4$@$SiO_2$ against $Hg^{2+}$, a titration experiment was performed and the results were shown in Fig. 6. For this purpose 0.03 g of nanocomposite was dispersed in 10 mL of 0, 0.1, 0.3, 0.5, 1, 3, 5, 10, 20, and 30 $\times$ $10^{-6}$ M of $Hg^{2+}$ in PBS buffer solution (pH = 7, water). As can be seen in Fig. 6a, with increasing $Hg^{2+}$ concentration, two appeared peaks at 409 nm (denoted as blue emission) and 351 nm (denoted as UV emission) are gradually quenched. It is clearly seen that the blue emission is quenched faster than the UV emission. It proves that the part of the fluorophore molecule which is responsible for the UV emission, is first involved in PET mechanism from $Hg^{2+}$ as the receptor. On the other hand, it seems that the receptor is directly bonded to the group(s) responsible for the blue emission and is transferring electron to this group(s) through PET mechanism[44] which results in a faster "turn-off". Fig. 6b shows the graph of fluorescence intensity *versus* $Hg^{2+}$ concentration. It is seen that in the range of 0.1–0.5 μM of $Hg^{2+}$, there is a good linear relationship in the graph with $R^2 = 0.9833$. The regression equation is $F = -1896.2C$ (μM $Hg^{2+}$) + 1225.5 for the intensity change of the red shift with increasing $Hg^{2+}$ concentration. The limit of detection (LOD) of the probe was calculated to be 48.7 nM for $Hg^{2+}$ detection which satisfies the U.S. EPA (the U.S. Environmental Protection Agency) limits (~2 ppb) of $Hg^{2+}$ detection in drinking water and is a good record compared to some other reports.[38,46–48]

The selectivity of the synthesized probe was tested in presence of some interfering ions. Fig. 7 shows the fluorescence

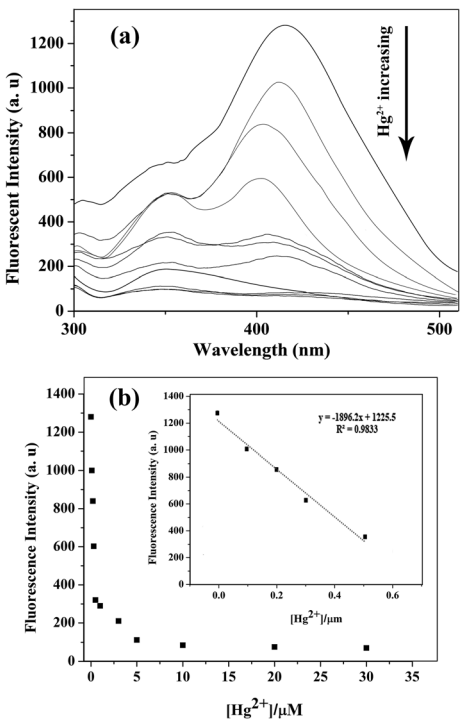


Fig. 6 (a) Fluorescence emission spectra ($\lambda_{exc}$ = 268 nm) of VBYT-$Fe_3O_4$@$SiO_2$ (1 $\times$ $10^{-6}$ M) in the presence of increasing concentrations of $Hg^{2+}$ (0–30 μM). (b) The change of the emission intensities at 409 nm with increasing $Hg^{2+}$ concentration.

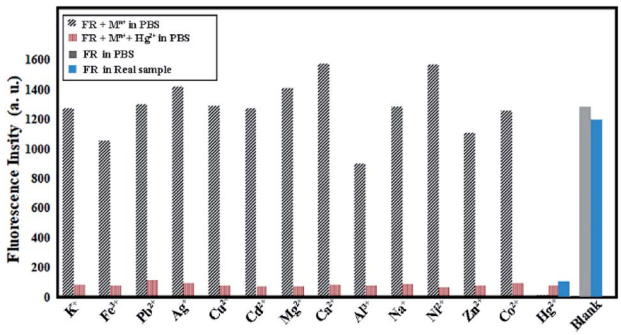


Fig. 7 Fluorescence response of VBYT-$Fe_3O_4$@$SiO_2$ to various interfering cations in aqueous solution. The concentrations of all the tested ions were 1 μM. The intensities were recorded at 409 nm, excitation at 268 nm, FR: free receptor.

changes of VBYT-$Fe_3O_4$@$SiO_2$ by treatment of $10^{-6}$ M of the interfering ions in 10 mL PBS buffer solution containing 0.03 g of the dispersed nanocomposite. Moreover, the interfering ions were tested in presence of the same concentration of $Hg^{2+}$. It is shown that the tested metal ions ($Na^+$, $K^+$, $Mg^{2+}$, $Al^{3+}$, $Ca^{2+}$, $Cd^{2+}$, $Ni^{2+}$, $Co^{2+}$, $Zn^{2+}$, $Cu^{2+}$, $Fe^{3+}$, $Pb^{2+}$, $Ag^+$) have small or no interference with $Hg^{2+}$ ions and this ion can be easily detected in presence of either of the shown elements. In order to have an account of the behaviour of the designed probe in the real sample, the fluorescence spectra of FR as well as FR plus $Hg^{2+}$ ions were tested in drinking tap water of University of Zabol as a real sample. The results shown in Fig. 7 (in blue columns) show that very similar behaviour is also observed in the real sample. These results suggest that VBYT-$Fe_3O_4$@$SiO_2$ is a good candidate to be applied for detection of $Hg^{2+}$ with high selectivity against other metal ions in a real aqueous samples.

To test the regeneration ability of the probe, VBYT-$Fe_3O_4$@$SiO_2$ was tested by using excess amount of NaI which is able to remove $Hg^{2+}$ from the chemosensor surface. Fig. 8 shows the results of the regeneration test which proves that the fluorescence properties of VBYT-$Fe_3O_4$@$SiO_2$ is reversible and the

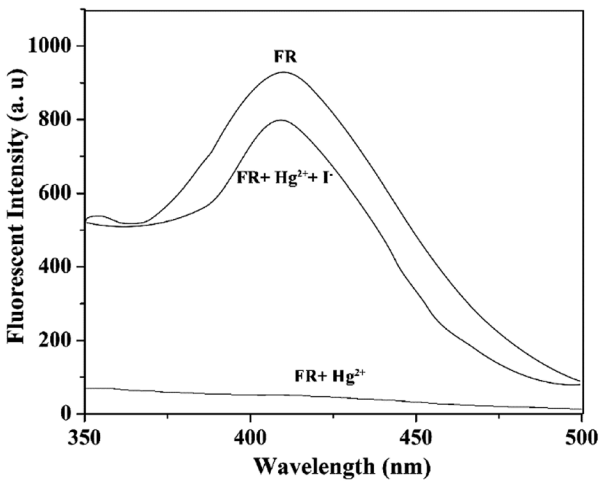


Fig. 8 Fluorescence spectra of top: FR (VBYT-$Fe_3O_4$@$SiO_2$), middle: FR plus $Hg^{2+}$ (1 $\times$ $10^{-6}$ M), and, bottom: FR and $Hg^{2+}$ plus $I^-$ (excess) in aqueous solution.

probe still has its ability after removing the content of $Hg^{2+}$ ions by NaI.

In the present study, interactions of the $Hg^{+2}$ ions with positions on VBYT–AEAPTES ligand which encompass nitrogen and sulphur atoms were considered. Results indicate that the $Hg^{+2}$ ions interact preferably with the ligand through atoms $N_{28}$, $N_{31}$, and $S_{37}$ which are labelled in Scheme 3. The binary complexes which was formed through interactions of the $Hg^{+2}$ ions with the mentioned atoms on the ligand are denoted as A, B, and C, respectively (see Scheme 3). The order of the binding energies of these complexes (in kcal $mol^{-1}$) is: B (217.61) < A (220.20) < C (227.75). Also, gaps between energies of highest occupied molecular orbital (HOMO) and lowest unoccupied molecular orbital (LUMO) in ligand and complexes were calculated. The results point out that energy gap in the ligand is 2.857 eV and interactions of $Hg^{+2}$ ions with the ligand lead to decreasing the energy gaps in the complexes. The order of energy gaps in the complexes (in eV) is: B (0.423) < A (0.432) < C (0.478) which is in agreement with the order of the binding energies.

The NBO analysis was performed on the mentioned complexes to obtain better insight regarding the order of binding energies. Donor–acceptor interaction energy ($E^2$) values between all donors and acceptors were studied. Results indicate that the order of $E^2$ values (in kcal $mol^{-1}$) of interactions between lone pair (Lp) of Hg and antibonding (BD*) orbitals of X–Y (X = $N_{28}$, $N_{31}$, and $S_{37}$; Y = $C_{11}$, $C_{32}$, and $C_{33}$) in the complexes is: C (0.36) < A (0.51) < B (0.74). In fact, decrease of anti-bonding feature of X–Y bonds through interaction of $Hg^{+2}$ ions with VBYT–AEAPTES ligand leads to increase of binding energies of the complexes.

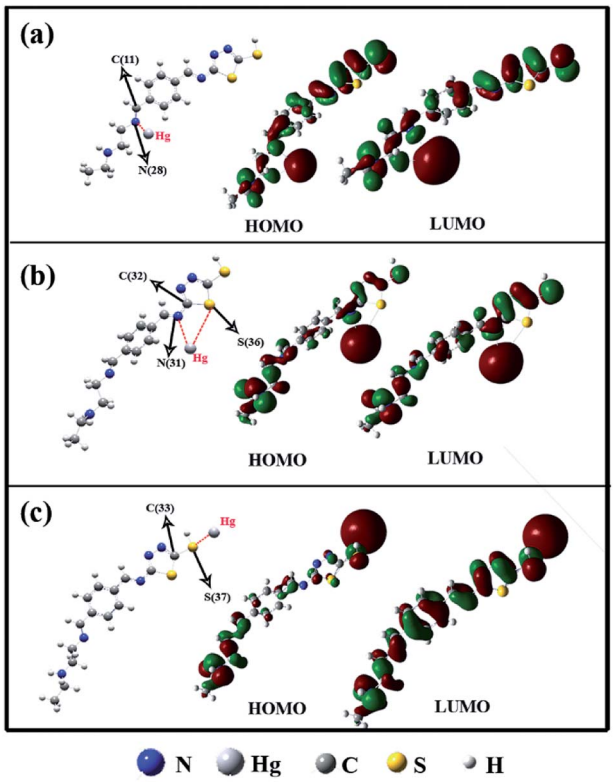


Scheme 3 Molecular orbital structure of HOMO and LUMO of different bonding modes including (a) $N_{28}$, (b) $N_{31}$ and $S_{36}$, and (c) $S_{37}$.

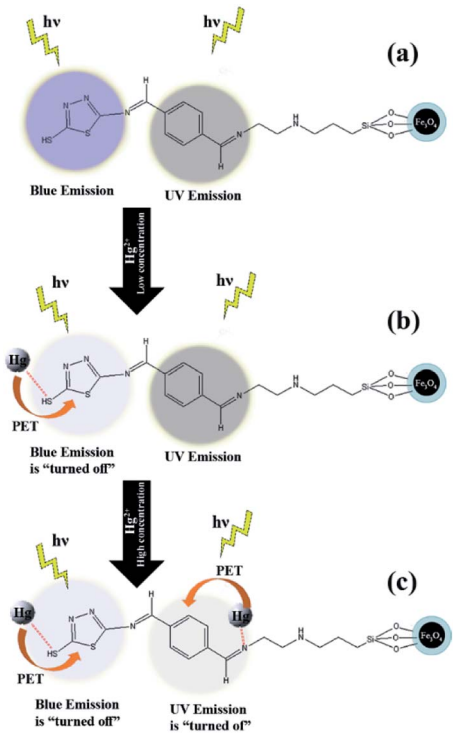


Scheme 4 The proposed mechanism for "turn-off" behavior of UV and blue emissions of VBYT-$Fe_3O_4$@$SiO_2$ after addition of $Hg^{2+}$ ions: (a) free receptor (b) after addition of low concentration of $Hg^{2+}$, (c) after addition of high concentration of $Hg^{2+}$.

Based on the abovementioned theoretical results, the fluorescence "turn-off" behaviour of VBYT-$Fe_3O_4$@$SiO_2$ nanocomposites is depicted in Scheme 4. As can be seen in Scheme 4a, two different parts of the VBYT molecule including benzylidene and thiadiazole are responsible for UV and blue emissions, respectively. After addition of low concentrations of $Hg^{2+}$, $S_{37}$ site coordinated to the entered metal ions due to its higher binding energy. The coordinated $Hg^{2+}$ ion may act as receptor and transfers electron to the fluorophore *via* PET mechanism causing the quenching of the blue emission (Scheme 4b). Another possible mechanism for quenching the UV band could be the enhanced intersystem crossing (ISC) to the triplet state due to "heavy ion effect".[49,50] By increasing the concentration of the $Hg^{2+}$ ions in the solution and saturation of $S_{37}$ sites in VBYT molecule, gradually $N_{28}$–$Hg^{2+}$ bond with high binding energy is formed and again, by PET mechanism, the UV emission turns off, as well. Quenching of blue emission due to the "heavy ion effect" is less likely since the sensor is already significantly spin–orbit coupled due to the already coordinated $Hg^{2+}$ ion.[44]

## Conclusions

VBYT-$Fe_3O_4$@$SiO_2$ nanocomposites were synthesized by using ATT as a starting material. The characterizations showed

successful synthesis of $Fe_3O_4$@$SiO_2$ and its functionalization with VBYT ligand. The prepared nanocomposite was easily separated from the solution by an external magnet. The fluorescence response of the nanocomposite against different ions showed that the blue fluorescence peak is easily quenched by adding $Hg^{2+}$ ions. The sensitivity of the probe was calculated by titration tests and it was shown that the limit of detection is 48.7 nm and the fluorescence intensity diagram against $Hg^{2+}$ concentration showed a good linear relationship in the range of 0.1–0.5 μM. Theoretical calculations showed that the binding energies of $S_{37}$, $N_{28}$, and $N_{31}$ bonds with $Hg^{2+}$ ion has an order of $S_{37} > N_{28} > N_{31}$. The presence of various active sites for coordination to mercury atoms makes this detector potential adsorbent for removing heavy metal atoms with high capacity. The absorbing application of the designed nanomaterial is the subject of our further research work.

## Conflicts of interest

There are no conflicts to declare.

## Acknowledgements

This work was supported by University of Zabol.

## Notes and references

1 U.S.E.U.S.E.P. Agency, *2011 National Emissions Inventory, technical support document. Draft report, Version 2*, 2015.
2 U.S. EPA, *Data from the 2011 National Emissions Inventory Version 1*, 2014.
3 J.-D. Park and W. Zheng, Human exposure and health effects of inorganic and elemental mercury, *Journal of Preventive Medicine & Public Health*, 2012, **45**(6), 344.
4 U. EPA, Mercury Update: Impact on Fish Advisories, *EPA Fact Sheet EPA-823-F-01-011*, 2001.
5 M. Ruiz-de-Cenzano, A. Rochina-Marco, M. L. Cervera and M. de la Guardia, Speciation of methylmercury in market seafood by thermal degradation, amalgamation and atomic absorption spectroscopy, *Ecotoxicol. Environ. Saf.*, 2014, **107**, 90–96.
6 H. Cheng, C. Wu, L. Shen, J. Liu and Z. Xu, Online anion exchange column preconcentration and high performance liquid chromatographic separation with inductively coupled plasma mass spectrometry detection for mercury speciation analysis, *Anal. Chim. Acta*, 2014, **828**, 9–16.
7 S. S. de Souza, A. D. Campiglia and F. Barbosa, A simple method for methylmercury, inorganic mercury and ethylmercury determination in plasma samples by high performance liquid chromatography–cold-vapor-inductively coupled plasma mass spectrometry, *Anal. Chim. Acta*, 2013, **761**, 11–17.
8 N. Wang, M. Lin, H. Dai and H. Ma, Functionalized gold nanoparticles/reduced graphene oxide nanocomposites for ultrasensitive electrochemical sensing of mercury ions based on thymine–mercury–thymine structure, *Biosens. Bioelectron.*, 2016, **79**, 320–326.
9 Z. Liu, W. He and Z. Guo, Metal coordination in photoluminescent sensing, *Chem. Soc. Rev.*, 2013, **42**(4), 1568–1600.
10 M. H. Keefe, K. D. Benkstein and J. T. Hupp, Luminescent sensor molecules based on coordinated metals: a review of recent developments, *Coord. Chem. Rev.*, 2000, **205**(1), 201–228.
11 X. Peng, Y. Wang, X. Tang and W. Liu, Functionalized magnetic core–shell $Fe_3O_4$@$SiO_2$ nanoparticles as selectivity-enhanced chemosensor for Hg(II), *Dyes Pigm.*, 2011, **91**(1), 26–32.
12 M. Shao, F. Ning, J. Zhao, M. Wei, D. G. Evans and X. Duan, Preparation of $Fe_3O_4$@$SiO_2$@Layered Double Hydroxide Core–Shell Microspheres for Magnetic Separation of Proteins, *J. Am. Chem. Soc.*, 2012, **134**(2), 1071–1077.
13 S. Thatai, P. Khurana, J. Boken, S. Prasad and D. Kumar, Nanoparticles and core–shell nanocomposite based new generation water remediation materials and analytical techniques: a review, *Microchem. J.*, 2014, **116**, 62–76.
14 Y. Zhou, L. Tang, G. Zeng, C. Zhang, Y. Zhang and X. Xie, Current progress in biosensors for heavy metal ions based on DNAzymes/DNA molecules functionalized nanostructures: a review, *Sens. Actuators, B*, 2016, **223**, 280–294.
15 F. Wang, Z. Gu, W. Lei, W. Wang, X. Xia and Q. Hao, Graphene quantum dots as a fluorescent sensing platform for highly efficient detection of copper(II) ions, *Sens. Actuators, B*, 2014, **190**, 516–522.
16 G. E. LeCroy, S. K. Sonkar, F. Yang, L. M. Veca, P. Wang, K. N. Tackett, J.-J. Yu, E. Vasile, H. Qian and Y. Liu, Toward structurally defined carbon dots as ultracompact fluorescent probes, *ACS Nano*, 2014, **8**(5), 4522–4529.
17 H.-S. Wang, C. Wang, Y.-K. He, F.-N. Xiao, W.-J. Bao, X.-H. Xia and G.-J. Zhou, Core–shell Ag@ $SiO_2$ nanoparticles concentrated on a micro/nanofluidic device for surface plasmon resonance-enhanced fluorescent detection of highly reactive oxygen species, *Anal. Chem.*, 2014, **86**(6), 3013–3019.
18 Y. Ding, W. Zhu, Y. Xu and X. Qian, A small molecular fluorescent sensor functionalized silica microsphere for detection and removal of mercury, cadmium, and lead ions in aqueous solutions, *Sens. Actuators, B*, 2015, **220**, 762–771.
19 G. Jha, N. Anoop, A. Rahaman and M. Sarkar, Fluoride ion sensing in aqueous medium by employing nitrobenzoxadiazole-postgrafted mesoporous silica nanoparticles (MCM-41), *Phys. Chem. Chem. Phys.*, 2015, **17**(5), 3525–3533.
20 Z. Dong, X. Tian, Y. Chen, J. Hou and J. Ma, Rhodamine group modified SBA-15 fluorescent sensor for highly selective detection of $Hg^{2+}$ and its application as an INHIBIT logic device, *RSC Adv.*, 2013, **3**(7), 2227–2233.
21 X. Guo, F. Mao, W. Wang, Y. Yang and Z. Bai, Sulfhydryl-modified $Fe_3O_4$@$SiO_2$ core/shell nanocomposite: synthesis and toxicity assessment *in vitro*, *ACS Appl. Mater. Interfaces*, 2015, **7**(27), 14983–14991.

22 U. Jeong, H. H. Shin and Y. Kim, Functionalized magnetic core–shell Fe@$SiO_2$ nanoparticles as recoverable colorimetric sensor for $Co^{2+}$ ion, *Chem. Eng. J.*, 2015, **281**, 428–433.

23 B. Zhu, J. Zhao, H. Yu, L. Yan, Q. Wei and B. Du, Naphthalimide-functionalized $Fe_3O_4$@$SiO_2$ core/shell nanoparticles for selective and sensitive adsorption and detection of $Hg^{2+}$, *Chem. Eng. J.*, 2013, **219**, 411–418.

24 L. Wang, J. Yan, W. Qin, W. Liu and R. Wang, A new rhodamine-based single molecule multianalyte ($Cu^{2+}$, $Hg^{2+}$) sensor and its application in the biological system, *Dyes Pigm.*, 2012, **92**(3), 1083–1090.

25 C. Wang, S. Tao, W. Wei, C. Meng, F. Liu and M. Han, Multifunctional mesoporous material for detection, adsorption and removal of $Hg^{2+}$ in aqueous solution, *J. Mater. Chem.*, 2010, **20**(22), 4635–4641.

26 L. Sun, Y. Li, M. Sun, H. Wang, S. Xu, C. Zhang and Q. Yang, Porphyrin-functionalized $Fe_3O_4$@$SiO_2$ core/shell magnetic colorimetric material for detection, adsorption and removal of $Hg^{2+}$ in aqueous solution, *New J. Chem.*, 2011, **35**(11), 2697–2704.

27 Y. Liu, R. Fu, Y. Sun, X. Zhou, S. A. Baig and X. Xu, Multifunctional nanocomposites $Fe_3O_4$@ $SiO_2$–EDTA for Pb(II) and Cu(II) removal from aqueous solutions, *Appl. Surf. Sci.*, 2016, **369**, 267–276.

28 X. Zhang, Y. Zhang, X. Zhang, S. Li and Y. Huang, Nitrogen rich core–shell magnetic mesoporous silica as an effective adsorbent for removal of silver nanoparticles from water, *J. Hazard. Mater.*, 2017, **337**, 1–9.

29 Y. Hu, C.-Y. Li, X.-M. Wang, Y.-H. Yang and H.-L. Zhu, 1,3,4-Thiadiazole: synthesis, reactions, and applications in medicinal, agricultural, and materials chemistry, *Chem. Rev.*, 2014, **114**(10), 5572–5610.

30 D. M. Kamiński, A. A. Hoser, M. Gagoś, A. Matwijczuk, M. Arczewska, A. Niewiadomy and K. Woźniak, Solvatomorphism of 2-(4-fluorophenylamino)-5-(2,4-dihydroxybenzeno)-1,3,4-thiadiazole chloride, *Cryst. Growth Des.*, 2010, **10**(8), 3480–3488.

31 A. Matwijczuk, D. Karcz, R. Walkowiak, J. Furso, B. Gładyszewska, S. Wybraniec, A. Niewiadomy, G. P. Karwasz and M. Gagoś, Effect of Solvent Polarizability on the Keto/Enol Equilibrium of Selected Bioactive Molecules from the 1,3,4-Thiadiazole Group with a 2,4-Hydroxyphenyl Function, *J. Phys. Chem. A*, 2017, **121**(7), 1402–1411.

32 A. A. Hoser, D. M. Kamiński, A. Matwijczuk, A. Niewiadomy, M. Gagoś and K. Woźniak, On polymorphism of 2-(4-fluorophenylamino)-5-(2,4-dihydroxybenzeno)-1,3,4-thiadiazole (FABT) DMSO solvates, *CrystEngComm*, 2013, **15**(10), 1978–1988.

33 D. M. Kamiński, A. Matwijczuk, D. Pociecha, E. Górecka, A. Niewiadomy, M. Dmowska and M. Gagoś, Effect of 2-(4-fluorophenylamino)-5-(2,4-dihydroxyphenyl)-1,3,4-thiadiazole on the molecular organisation and structural properties of the DPPC lipid multibilayers, *Biochim. Biophys. Acta, Biomembr.*, 2012, **1818**(11), 2850–2859.

34 A. Matwijczuk, D. Kamiński, A. Górecki, A. Ludwiczuk, A. Niewiadomy, S. Maćkowski and M. Gagoś, Spectroscopic Studies of Dual Fluorescence in 2-((4-Fluorophenyl)amino)-5-(2,4-Dihydroxybenzeno)-1,3,4-Thiadiazole, *J. Phys. Chem. A*, 2015, **119**(44), 10791–10805.

35 N. Mir, A. Heidari, H. Beyzaei, S. Mirkazehi-Rigi and P. Karimi, Detection of $Hg^{2+}$ in aqueous solution by pyrazole derivative-functionalized $Fe_3O_4$@$SiO_2$ fluorescent probe, *Chem. Eng. J.*, 2017, **327**, 648–655.

36 A. Heidari and N. Mir, 4-Acetamidobenzaldehyde-Functionalized $Fe_3O_4$@$SiO_2$ Fluorescent Nanocomposite Probe for Detection of $Hg^{2+}$ in Aqueous Solution, *J. Fluoresc.*, 2017, **27**(2), 659–667.

37 P. Tzvetkova, P. Vassileva and R. Nickolov, Modified silica gel with 5-amino-1,3,4-thiadiazole-2-thiol for heavy metal ions removal, *J. Porous Mater.*, 2010, **17**(4), 459–463.

38 Z. Dong, X. Tian, Y. Chen, Y. Guo and J. Ma, Dansyl derivative functionalized $Fe_3O_4$@$SiO_2$ fluorescent probe for detection and removal of $Hg^{2+}$ in aqueous solution, *RSC Adv.*, 2013, **3**(4), 1082–1088.

39 M. Frisch, G. Trucks, H. B. Schlegel, G. Scuseria, M. Robb, J. Cheeseman, G. Scalmani, V. Barone, B. Mennucci, G. Petersson, *Gaussian 09, revision a. 02*, Gaussian, Inc., Wallingford, CT 200, 2009.

40 E. Glendening, A. Reed, J. Carpenter and F. Weinhold, *NBO Version 3.1, TCI*, University of Wisconsin, Madison 65, 1998.

41 A. E. Reed, L. A. Curtiss and F. Weinhold, Intermolecular interactions from a natural bond orbital, donor–acceptor viewpoint, *Chem. Rev.*, 1988, **88**(6), 899–926.

42 C. L. Garcia and J. A. Lercher, Adsorption and surface chemistry of light thiols on Na-ZSM5 and H-ZSM5, *J. Phys. Chem.*, 1991, **95**(26), 10729–10736.

43 L. N. Neupane, J.-Y. Park, J. H. Park and K.-H. Lee, Turn-on Fluorescent Chemosensor Based on an Amino Acid for Pb(II) and Hg(II) Ions in Aqueous Solutions and Role of Tryptophan for Sensing, *Org. Lett.*, 2013, **15**(2), 254–257.

44 A. P. De Silva, H. N. Gunaratne, T. Gunnlaugsson, A. J. Huxley, C. P. McCoy, J. T. Rademacher and T. E. Rice, Signaling recognition events with fluorescent sensors and switches, *Chem. Rev.*, 1997, **97**(5), 1515–1566.

45 X.-C. Fu, J. Wu, C.-G. Xie, Y. Zhong and J.-H. Liu, Rhodamine-based fluorescent probe immobilized on mesoporous silica microspheres with perpendicularly aligned mesopore channels for selective detection of trace mercury(II) in water, *Anal. Methods*, 2013, **5**(10), 2615–2622.

46 H. Wang, Y. Li, S. Xu, Y. Li, C. Zhou, X. Fei, L. Sun, C. Zhang, Y. Li, Q. Yang and X. Xu, Rhodamine-based highly sensitive colorimetric off-on fluorescent chemosensor for $Hg^{2+}$ in aqueous solution and for live cell imaging, *Org. Biomol. Chem.*, 2011, **9**(8), 2850–2855.

47 Y. Xu, Y. Zhou, W. Ma, S. Wang and S. Li, Functionalized magnetic core–shell $Fe_3O_4$@$SiO_2$ nanoparticles for sensitive detection and removal of $Hg^{2+}$, *J. Nanopart. Res.*, 2013, **15**(6), 1–9.

 

48 C.-l. Fang, J. Zhou, X.-j. Liu, Z.-h. Cao and D.-h. Shangguan, Mercury(II)-mediated formation of imide–Hg–imide complexes, *Dalton Trans.*, 2011, **40**(4), 899–903.

49 D. S. McClure, Triplet–Singlet Transitions in Organic Molecules. Lifetime Measurements of the Triplet State, *J. Chem. Phys.*, 1949, **17**(10), 905–913.

50 A. K. Singh, S. K. Singh, H. Mishra, R. Prakash and S. B. Rai, Structural, Thermal, and Fluorescence Properties of Eu(DBM)3Phenx Complex Doped in PMMA, *J. Phys. Chem. B*, 2010, **114**(41), 13042–13051.